

GreedyFool: An Imperceptible Black-box Adversarial Example Attack against Neural Networks

Hui Liu

Wuhan University
Penn State University

Bo Zhao

Wuhan University

Jiabao Guo

Wuhan University

Yang An

Wuhan University

Peng Liu

Penn State University

Abstract—Deep neural networks (DNNs) are inherently vulnerable to well-designed input samples called adversarial examples. The adversary can easily fool DNNs by adding slight perturbations to the input. In this paper, we propose a novel black-box adversarial example attack named GreedyFool, which synthesizes adversarial examples based on the differential evolution and the greedy approximation. The differential evolution is utilized to evaluate the effects of perturbed pixels on the confidence of the DNNs-based classifier. The greedy approximation is an approximate optimization algorithm to automatically get adversarial perturbations. Existing works synthesize the adversarial examples by leveraging simple metrics to penalize the perturbations, which lack sufficient consideration of the human visual system (HVS), resulting in noticeable artifacts. In order to sufficient imperceptibility, we launch investigations into the HVS and design an integrated metric considering just noticeable distortion (JND), Weber-Fechner law, texture masking and channel modulation, which is proven to be a better metric to measure the perceptual distance between the benign examples and the adversarial ones. The experimental results demonstrate that GreedyFool has several remarkable properties including black-box, 100% success rate, flexibility, automation and can synthesize the more imperceptible adversarial examples than the state-of-the-art pixel-wise methods.

Keywords—Deep neural networks, adversarial examples, differential evolution, greedy approximation, human visual system

I. INTRODUCTION

Deep neural networks (DNNs) [1-3] have demonstrated impressive performance in wide application, e.g., image processing [4, 5], nature language processing [6, 7], speech recognition [8, 9], etc. Especially in the field of image classification, DNNs-based approach achieves even human-competitive results. These applications have a common characteristic: the adversary is able to impersonate an benign user to precisely control the input to DNNs-based services. However, recent studies found that DNNs are inherently vulnerable to well-designed input samples called adversarial examples. The attackers can easily fool DNNs by adding slight perturbations to the benign examples. Such attacks are a serious threat for those safety-critical systems, such as facial biometric systems [10], digital watermarking [11], etc. For example, the attacker who wears a pair of perturbed eyeglass frames could evade being recognized or impersonate another individual by the state-of-the-art face-recognition algorithm. In digital watermarking field, the adversarial perturbations could impact the integrity of the embedded pattern, making the watermark undetectable and the authenticity of the digital media unverifiable. The phenomena of adversarial example attacks have aroused great concern from academia and industry.

In image classification tasks, adversarial example attacks aim to mislead the DNNs-based classifier to the modified

image as a wrong or specific target class. Generating adversarial examples could be formalized as an optimization problem with constrains. This problem involves two aspects: how to solve for this optimal solution and how to define the perceptual loss.

Due to non-linear and non-convex of the DNN model, optimization problem of adversarial examples is difficult to solve. In recent years, many advanced solutions have been proposed. Szegedy C et al. [12] first revealed the sensitivity to well-designed perturbation which can be crafted by several gradient-based algorithms using back-propagation for obtaining gradient information. Specifically, Goodfellow I.J et al. [13] proposed the fast gradient sign method (FGSM) to yield a simple and fast method of generating adversarial examples based on a hypothesis in which the linearity and high-dimensions of inputs are the main reason why a broad class of networks are sensitive to small perturbation. Jacobian-based saliency map attack [14] is an efficient method to generate adversarial examples using forward-propagation, which compute the Jacobian of the input example and construct adversarial saliency maps to evaluate the effect of perturbed features. These approaches that require inner information of target DNNs, including gradient information and network structures, cannot be applied to black-box attack scenarios. In one-pixel attack [15], Su J et al. proposed a black-box method for generating one-pixel adversarial perturbations based on the differential evolution, which requires only probability labels but no inner information of target DNNs and can attack more types of DNNs. However, when synthesizing adversarial examples, the attackers have no way of knowing in advance how many pixels may be perturbed, resulting in the failure of adversarial example attacks toward some images.

In terms of the perceptual loss, most of the existing attacks utilize perceptual distance of L_p norms (L_0 , L_2 and L_∞ norms) as constraint to penalize the perturbations. For example, Papernot N et al. [16] generated adversarial examples based on a precise understanding of the mapping between inputs and outputs of DNNs by L_2 norm. FGSM [13] computed one-step gradient to synthesize adversarial examples by L_∞ norm. Carlini N et al. [17] used three distance metrics L_0 , L_2 and L_∞ to quantify similarity. These metrics treat perturbations of different pixels in an image equally important for human eyes. However, visibility of perturbations is the perceived response by the individual to the physical stimulus. The measurement of the perceptual distance between the benign examples and the adversarial ones should take full consideration of the human visual system (HVS). Therefore, we launch a lot of investigations into the HVS and summarize four primary factors affecting the human vision: (a) Just noticeable distortion (JND) [18, 19]. Human eyes cannot sense a stimulus below the JND, which quantifies the sensitivity of the HVS to different background luminance. (b) Weber-Fechner law [20, 21]. The HVS is sensitive to luminance contrast rather than absolute luminance value. The Weber-Fechner law revealed

important principle in psychophysics, which describes the logarithmic mapping between the magnitude of a physical stimulus and its perceived intensity. (c) Texture masking [22]. Imperceptibility of perturbations is caused by an increase in the texture non-uniformity in the neighborhood. Human eyes are more sensitive to perturbations on pixels in smooth regions than those in textured regions. (d) Channel modulation [23, 24]. The strength of the signal in each channel would be proportional to the sensitivity of the human eye. And human vision has different sensitivity to the same perturbation in different color channels. These factors reveal the sensitivity of human eyes to pixel perturbations from four different aspects. There are many works introducing the HVS to quantify the perceptual loss. A typical work is that Luo B [22] defined perturbation sensitivity distance (PSD), taking the HVS into consideration, to measure perceptual distance between the benign examples and the adversarial ones. This method ignores the logarithmic mapping between the physical magnitude and its perceived intensity, and lacks consideration of the discrimination in different color channels. Our work integrates JND, Weber-Fechner law, texture masking and channel modulation and design a better metric to measure the perceptual loss caused by adversarial perturbations.

In this paper, we focus on the approach of synthesizing adversarial examples and the definition of the perceptual loss. To synthesize adversarial examples with no inner information of target DNNs, we apply the differential evolution [15, 25, 26] to evaluate the effects of perturbed pixels on the confidence of target DNNs and introduce the greedy approximation [22] to automatically find which pixels to perturb and what magnitude to modify effectively. In terms of the perceptual loss, previous related works used simple metrics to evaluate the perceptual distances between the benign examples and the adversarial ones, which could be easily detected by human eyes. We investigate the HVS and summarize four primary factors (JND, Weber-Fechner law, texture masking and channel modulation) affecting the human vision. Furthermore, we propose a comprehensive metric considering the HVS to evaluate the perceptual similarity between the benign examples and the adversarial ones. The experimental results prove that GreedyFool can effectively synthesize the adversarial examples with low visibility and high success rate.

The paper makes the following contributions:

(1) We propose a black-box adversarial example attack approach GreedyFool, which requires only the feedback of the DNNs-based classifier but no inner information of target DNNs. Thus, GreedyFool can attack more types of DNNs even if they are not differentiable.

(2) We design a forward-propagation based on the differential evolution and the greedy approximation to carry out adversarial example attack. The differential evolution to evaluate the effects of pixel-wise perturbation and generate candidates with the higher perturbation priority, combining with the greedy approximation to automatically find which pixels to perturb and what magnitude to add. The proposed method achieves 100% success rate for non-targeted attacks and targeted attacks.

(3) We design an integrated metric considering JND, Weber-Fechner law, texture masking and channel modulation of the HVS to evaluate the perceptual distances between the benign examples and the adversarial ones. The experimental

results show that the proposed perceptual loss is a better metric than the exiting pixel-wise metrics.

The remainder of this paper is organized as follows. We present the preliminaries in Section II and give the careful investigation into the HVS in Section III. In Section IV, we give details about the design and the implementation of GreedyFool. The experimental evaluations are presented in Section V. Finally, we discuss several remarkable properties of GreedyFool in Section VI and conclude the paper in Section VII.

II. PRELIMINARIES

A. Deep Neural Network

Deep neural network [1-3] is usually constructed by multiple neural network layers, which would be convolutional layers, pooling layers and fully connected layers as in convolutional neural network. A neural network layer consists of a set of perceptrons and each perceptron has multiple inputs and one output with an activation function, e.g., Sigmoid, ReLU. It can be formalized in a chain.

$$f(x, \theta) = f^{(k)}(\dots f^{(2)}(f^{(1)}(x, \theta_1), \theta_2), \theta_k) \quad (1)$$

where $f^{(i)}(x, \theta_i)$ is the function of the i 'th layer of the network, $i = 1, 2, \dots, k$. x is the input example and θ_i is the weight of the i 'th layer.

Among neural network architectures, residual network (ResNet) [2] and dense convolutional network (DenseNet) [3] are two types of widely used neural networks in image classification tasks. Instead of learning unreference functions, ResNet reformulates the layers as learning residual functions with reference to the layer inputs. A residual block is realized by feed-forward neural networks with “shortcut connections” shown in Fig. 1.

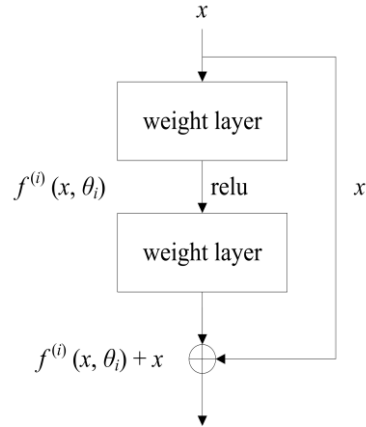


Fig. 1. A building block of residual learning. Shortcut connections are those skipping one or more layers.

We construct and train ResNet as described in TABLE I, which has 470,218 parameters and performs 92.69% accuracy in CIFAR-10.

To further improve the information flow between layers, DenseNet connects each layer to every other layer in a feed-forward fashion. Layers between dense blocks are named as transition layers and change feature-map sizes via convolution and pooling. DenseNet model has 850,606 parameters and performs 94.28% accuracy in CIFAR-10, whose structure is described in TABLE II.

TABLE I. THE STRUCTURE OF RESNET MODEL.

Layer	Parameters
Convolution layer 1	kernel = 3, stride = 1, depth = 16
Residual block 1	$[3 \times 3, 16] \times 5$
Residual block 2	$[3 \times 3, 32] \times 5$
Residual block 3	$[3 \times 3, 64] \times 5$
Global average pool	
Softmax classifier	

TABLE II. THE STRUCTURE OF DENSENET MODEL.

Layer	Parameters
Convolution layer 1	kernel = 3, stride = 1, depth = 24s
Dense block 1	$[1 \times 1, 48] \times 16$
Transition layer 1	Convolution layer (kernel = 1, stride = 1, depth = 12) Average pooling layer (kernel = 2, stride = 2)
Dense block 2	$[1 \times 1, 48] \times 16$
Transition layer 2	Convolution layer (kernel = 1, stride = 1, depth = 12) Average pooling layer (kernel = 2, stride = 2)
Dense block 3	$[1 \times 1, 48] \times 16$
Transition layer 3	Convolution layer (kernel = 1, stride = 1, depth = 12) Average pooling layer (kernel = 2, stride = 2)
Global average pool	
Softmax classifier	

B. CIFAR-10

The CIFAR-10 dataset consists of 60,000 $32 \times 32 \times 3$ color images, including 50,000 training images and 10,000 test images. It has 10 classes, including airplane, automobile, bird, cat, deer, dog, frog, horse, ship and truck, with 6,000 images per class. Due to its simplicity and small size, CIFAR-10 is easy to attack and defend. Therefore, CIFAR-10 is one of the most widely used image datasets to evaluate adversarial example attacks. In the paper, we adopt CIFAR-10 for the experiments and analyses.

C. Adversarial Example Attacks

Adversarial example attacks aim to mislead deep neural networks to an incorrect label by adding small perturbations in the benign examples, even if the perturbations are barely recognizable by human eyes. Adversarial examples [1, 19] would be formulated as a box-constrained optimization problem. That is,

$$\begin{aligned}
 & \min \|\delta\|_p \\
 & \text{s.t. } f(X') = l' \\
 & \quad f(X) = l \\
 & \quad l' \neq l \\
 & \quad X' = X + \delta \in D
 \end{aligned} \tag{2}$$

where a trained DNN model f predicts the benign example X and the adversarial example X' into l and l' . $\|\cdot\|$ denotes the perceptual distance between two examples, δ denotes the perturbation matrix added to the benign example for synthesizing the adversarial one, that remains in the benign domain D . This optimization problem minimizes the perturbation while misleading the DNN model to incorrect prediction.

D. Perceptual Distance

The perceptual distance is utilized to measure the perceptual similarity between the benign image and the adversarial image. Existing works mainly apply L_p norms (e.g. L_0 , L_2 and L_∞) to measure the magnitude of perturbation δ [1, 16, 17]. That is,

$$\|\delta\|_p = \left(\sum_{i=1}^n |\delta_i|^p \right)^{\frac{1}{p}} \tag{3}$$

where L_0 norm counts the number of pixels perturbed in an image. L_2 measures the Euclidean distance between the benign example and the adversarial example. L_∞ norm denotes the maximum for all vector elements $|\delta_i|$: $\|\delta\|_\infty = \max(|\delta_i|)$. The small L_p norm value indicates the more imperceptibility of perturbations. These metrics are objective, which treat perturbations of different pixels equally in an image. In fact, imperceptibility is the perceived response by the individual to the physical stimulus. Therefore, the mapping between physical stimulus and psychological perception should be fully considered in perceptual distance.

E. Differential Evolution

Differential evolution [15, 25, 26] is a population-based optimization algorithm for solving complex optimization problems. By remembering individual optimal solution and sharing information within the population, the differential evolution solves the optimization problem through cooperation and competition among individuals within the population. The differential evolution is a simple real parameter optimization based on mutation, crossover and selection. Figure 2 presents its mechanism through a simple cycle of stages.

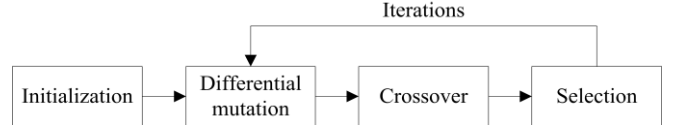


Fig. 2. Main stage of the differential evolution includes mutation, crossover and selection.

Due to non-linear and non-convex characteristics of the DNN model f , the Equation (2) is difficult to solve. It is proved that the differential evolution could efficiently find global optima than gradient-based methods or even other kinds of evolution algorithms [25]. The differential evolution is defined in Equation (4).

$$x_i(g+1) = x_{r1}(g) + F(x_{r2}(g) - x_{r3}(g)), \quad r1 \neq r2 \neq r3 \tag{4}$$

where $r1$, $r2$, $r3$ are random numbers and F is the scale parameter set to 0.5. Three candidate solutions $x_{r1}(g)$, $x_{r2}(g)$ and $x_{r3}(g)$ from the g 'th generation are randomly chosen to generate a new candidate solution $x_i(g+1)$ of the $g+1$ 'th generation. In this paper, the initial number of candidate solutions is 300, and at each iteration, another 300 candidate solutions will be produced by the differential evolution formula. The differential evolution neither requires the inner information of target DNNs, such as gradient information and network structures, nor requires the optimization problem to be differential as is required by classical optimization methods, e.g., gradient descent, quasi-newton, etc. These inherent features of the differential

evolution make GreedyFool flexible, which is applicable to more types of DNNs as a black-box attack tool.

III. HUMAN VISUAL SYSTEM

Human visual system is a multichannel model with characteristics of multi-frequency channel decomposition. Especially, the sensitivity of human eyes to perturbations is affected by several factors. We investigate the HVS and summarize four primary factors affecting the human vision in the image domain: JND, Weber-Fechner law, texture masking and channel modulation.

A. Just Noticeable Distortion

Human eyes cannot perceive a stimulus below the just noticeable distortion [18, 19] threshold around a pixel in images. The sensitivity of human eyes to noise of images has negative correlation with JDN. The larger value of the JDN threshold indicates the more noise can be hidden. An appropriate JND model can significantly improve the performance in image processing tasks. The visibility threshold of the JND is formulated in Equation (5), curved in Fig. 3.

$$jnd(x, y) = \begin{cases} 17(1 - \sqrt{\frac{\bar{I}_{n \times n}(x, y)}{127}}) + 3, & \text{if } \bar{I}_{n \times n}(x, y) \leq 127 \\ \frac{3}{128}(\bar{I}_{n \times n}(x, y) - 127) + 3, & \text{otherwise} \end{cases} \quad (5)$$

where $\bar{I}_{n \times n}(x, y)$ denotes the maximum luminance among a $n \times n$ window at the coordinate (x, y) . Especially, we set $n = 3$ and calculate the maximum luminance of the (x, y) pixel and its 8 neighbors.

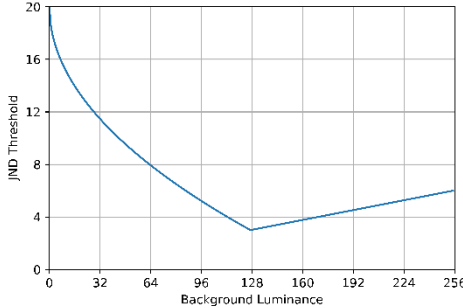


Fig. 3. Illustration of the JND. When the maximum luminance is 127, the JND threshold gets a minimum 3.

Figure 3 reveals the nonlinear relationship between the JND threshold and the maximum background luminance. Even if the magnitude of perturbations is the same, there are significant differences in perceived intensity of human eyes



Fig. 4. Perceptual distance of the perturbations with the same magnitude in different regions. The green line box marks perturbations in perturbed images. (a) benign example, (b) perturbed image at textured regions, (c) perturbed image at smooth regions.

under different luminance backgrounds. When the maximum luminance among a $n \times n$ window lies in the interval $[0, 127]$, the JDN threshold decreases as the background luminance increases. When the maximum luminance among a $n \times n$ window lies in the interval $[127, 255]$, the JDN threshold increases as the background luminance increases. If the maximum luminance is 127, the JDN threshold gets a minimum value 3. That indicates the perturbation at this coordinate is most easily perceived by the human eye.

B. Weber-Fechner Law

Weber-Fechner law [20, 21] has been proposed in the field of psychophysics to quantify relationships between any stimulus and the perceived response by individuals. The Weber law asserts that the just noticeable stimulus difference ΔI maintains a constant ratio with respect to the intensity of the comparison stimulus I . That is to say, if I is the intensity to which human eyes are adapted, and ΔI the increase in that intensity which is just perceptible, then the ratio $\frac{\Delta I}{I}$ may be considered as a measure of the discriminating power of human eyes. Furthermore, on the assumption that the difference threshold represents a unit change in sensation ΔS , Fechner defined Weber's law as:

$$\Delta S = k \frac{\Delta I}{I} \quad (6)$$

Integrating this formula, a logarithmic relation called the psychophysical law is generated, as shown in Equation (7).

$$S = k \ln I + C \quad (7)$$

where k and C are hyper parameters, I denotes the magnitude of a physical stimulus and S denotes the corresponding perceived intensity. The Weber-Fechner law revealed the logarithmic mapping between the magnitude of a physical stimulus and its perceived intensity, rather than absolute magnitude value as demonstrated in [22].

C. Texture Masking

According to texture masking theory [22], human eyes are more sensitive to perturbations on pixels in smooth regions than those in textured regions. We add 3×3 window perturbations with 100 magnitudes in the smooth region and the textured region respectively for comparison of perceptual distance. Figure 4 plots the benign example, perturbed image at textured regions and perturbed image at smooth regions from left to right. When perturbations with the same magnitude are added to the image, the perturbations in smooth regions are easy to be detected by human eyes, while those in textured regions are difficult to be recognized.

The standard deviation is a commonly used quantity to measure the texture masking of an image, which is proved to be effective in evaluating the perceptual loss of adversarial examples. The paper computes the standard deviation of a pixel p_i among an $n \times n$ window as shown in Equation (8).

$$SD(p_i) = \sqrt{\frac{\sum_{p_i \in S_i} (p_i - \mu)^2}{n^2}} \quad (8)$$

where S_i is the set consisting of pixels in the $n \times n$ window, μ is the average value of pixels in the region. The standard deviation $SD(p_i)$ is the variance of a pixel p_i among S_i . In the paper, we set $n = 3$ and calculate the standard deviation of the pixel p_i and its 8 neighbors. The texture masking reveals the close relationship between the perceptual loss and the local

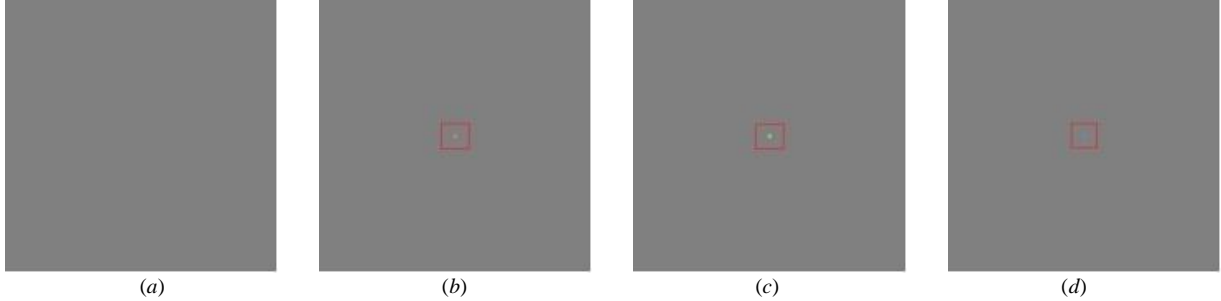


Fig. 5. Perceptual distance of the perturbations with the same magnitude in different channels. (a) benign example, (b) perturbed example in the red channel, (c) perturbed example in the green channel (d) perturbed example in the blue channel. The red Line box marks perturbations in perturbed examples.

We introduce the channel modulation to quantify the weight of perturbations in three color channels. The channel modulation is referred to a constrained linear combination of red, green and blue channels based on decolorization theory [24], which is formulated in Equation (9) for CIFAR-10.

$$\begin{aligned} \varpi &= \chi_r I_r + \chi_g I_g + \chi_b I_b \\ \text{s.t. } \chi_r + \chi_g + \chi_b &= 1 \\ \chi_r \geq 0, \chi_g \geq 0, \chi_b \geq 0 & \end{aligned} \quad (9)$$

where I_r , I_g and I_b are red, green and blue channels respectively, and ϖ is the result of the channel modulation. The non-negative numbers χ_r , χ_g and χ_b are channel weights that sum to 1. In the classical RGB2GRAY conversion model [24], the weights are fixed as $\{\chi_r = 0.299, \chi_g = 0.587, \chi_b = 0.114\}$. In fact, a more flexible scheme would be fixing channel weights depending on input images and individuals.

IV. METHODOLOGY

Adversarial example attacks could be formulated as an optimization problem with constraints. This problem involves the definition of the perceptual loss and the solution for the optimal problem. In the section, we describe in detail the definition of the perceptual loss and present a forward-propagation combining the differential evolution with the greedy approximation to solve for adversarial perturbations.

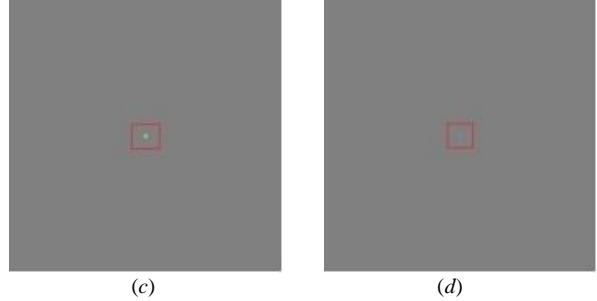
A. Perceptual Loss

In the investigation into the HVS, we find that the perceptual loss is primarily affected by four factors, namely JND, Weber-Fechner law, texture masking and channel

texture feature of the image. The region with the high standard deviation could hide more perturbations in an image.

D. Channel Modulation

According to spectral sensitivity theory [23, 24], the brain computes visual color by analyzing the relative excitations of three types of retinal cones, which is a specialized light-sensitive cell found in the retina of the eye and used for discrimination of color. Human eyes consist of red, green and blue cone cells, cone sensitized to different ranges of wavelength to provide a range of color perception. Due to differences in the number of cone cells, the human eyes are the most sensitive to green, followed by red, and the least sensitive to blue. We conduct the perturbations with the same magnitude in three color channels respectively. As shown in Fig. 5, the test prove that there are differences in the sensitivity of human eyes to color channels.



modulation. Weber-Fechner law reveals nonlinear relationships between any stimulus and the perceived response by individuals. In computer vision, the application of this law needs to consider the difference in perceived intensity of human eyes under different luminance backgrounds. The visibility of human eyes to perturbations of images has a positive correlation with stimulus and a negative correlation with JND. Thus, we combine Equation (5) and (6) to get a new quantity considering the perturbation intensity and the background luminance, as shown in Equation (10).

$$\Delta Ps = k \frac{\Delta I}{JND(I)} \quad (10)$$

where k is a constant according to Weber-Fechner law, ΔI is the just noticeable stimulus difference and ΔPs is a corresponding change in visual sensation. Since $JND(I)$ is a discrete piecewise function, we sum over the Equation (10) rather than integrate, as shown in Equation (11).

$$Ps(I) = k \sum_{i=I_0}^{I-1} \frac{1}{JND(i)} + C \quad (11)$$

where $Ps(I)$ is perceptual stimulus and I_0 is background luminance, k and C are constants. For the CIFAR-10 dataset, the pixel value ranges from 0 to 255 and the minimum difference between them is 1. For constructing the mapping between a physical stimulus and its perceptual stimulus, we define the perceptual stimulus in the interval $[0, 255]$. Obviously, a perturbation of magnitude 0 do not cause any perceptual perception to human eyes and a perturbation of magnitude 255 could cause the most noticeable perceptual perception. Thus, an equation could be constructed as follows to compute the constants k and C . That is,

$$\begin{cases} Ps(0) = C = 0, & \text{if } I = 0 \\ Ps(255) = k \sum_{i=0}^{255} \frac{1}{JND(i)} + C = 255, & \text{if } I = 255 \end{cases} \quad (12)$$

By solving the Equation (12), we get the parameter $C = 0$

$$\text{and } k = \frac{256}{\sum_{i=0}^{255} \frac{1}{JND(i)}}.$$

Texture masking reflects that perturbations at the region with high standard deviation are more imperceptible for human eyes than low standard deviation. The visibility of human eyes to perturbations has a negative correlation with the standard deviation of the region in an image. Furthermore, taking channel modulation into consideration, the definition of the perceptual loss fixes color channel weights according to decolorization theory. Thus, we propose an integrated metric to evaluate the perceptual loss as follow.

$$\text{IntegLoss}(p_i) = \sum_{c \in (r, g, b)} \chi_c \frac{Ps_c(p_i)}{SD_c(p_i)} \quad (13)$$

Adversarial example attacks usually add multiple pixel perturbations for success rate. The perceptual loss between the benign image and the adversarial one is the sum of the all pixel-wise perceptual loss. Therefore, we sum up all pixel-wise perceptual loss as follow.

$$\text{IntegLoss}(X, X') = \sum_{i=1}^N \sum_{c \in (r, g, b)} \chi_c \frac{Ps_c(p_i)}{SD_c(p_i)} \quad (14)$$

where N is the number of perturbed pixels in a benign image. $\text{IntegLoss}(X, X')$ denotes the perceptual loss integrating JND, Weber-Fechner law, texture masking and channel modulation between the benign example X and the adversarial one X' . The small IntegLoss value indicates the high perceptual similarity between the benign example and the adversarial one.

B. Pixel-wise Objective Function

State-of-the-art adversarial example attacks should allow DNNs to give the wrong output with a high confidence score by adding as little perturbations as possible. Therefore, we should choose these pixels that can reduce the confidence of DNNs in the true class or increase that in the target class with the less perceptual loss. The pixel-wise objective function called perturbation priority is defined to estimate the effect of perturbing a pixel as follow.

$$\text{PertPriority}(p_i) = \zeta \frac{P_t(X) - P_t(X')}{\text{IntegLoss}(p_i)} \quad (15)$$

where P_t denotes the probability that the example belongs to the label t . The adversarial example X' is synthesized by changing a pixel p_i of the benign example X . When $t = l$, setting $\zeta = 1$ and non-targeted attacks are executed, otherwise setting $\zeta = -1$ and targeted attacks are executed. Perturbation priority quantify the effects of the current pixel p_i perturbation on the confidence of the DNNs-based classifier in the target class. The bigger values of the perturbation priority are, the greater effects of the perturbations are.

C. Implementation

For finding out the pixels with high perturbation priority, the adversary has to choose which pixels to modify and what magnitudes to add for high misclassification ratio and low

imperceptibility. We encode the pixel-wise perturbation into an array as candidate solution (x, y, r, g, b) , which contains five elements: x - y coordinates and RGB value of the perturbation. A brute-force approach has to search all dimensions and pixel values for the optimal one. However, through this method the time taken for solving the problem is prohibitively long. To reduce the search time, we introduce the differential evolution referred in subsection II-E to solve the optimal of the pixel-wise objective function as the fitness function. For CIFAR-10 GreedyFool sets the total population size to be 300 and the number of generations $maxIter$ to be 60 for obtaining 18,000 candidate solutions with perturbation priority. And then the greedy approximation is utilized to automatically get a set of perturbed pixels and synthesize the imperceptible adversarial example. The implementation of GreedyFool is presented in Algorithm 1.

Algorithm 1: The Implementation of GreedyFool

Input: The original image X , the initial parameters of the differential evolution

Output: Adversarial example X'

- 1 **for** $i = 0$ to $maxIter$ **do**:
- 2 Calculate perturbation priority $PertPriority$ of all candidate solutions by the differential evolution and obtain a set $Pp = \{(unit_1, PertPriority_1), (unit_2, PertPriority_2), \dots\}$, where $unit_i = (x_i, y_i, r_i, g_i, b_i)$
- 3 **end for**
- 4 Sort Pp with $PertPriority$ in descending order to obtain a set $Sp = \{(unit'_1, PertPriority'_1), (unit'_2, PertPriority'_2), \dots\}$, where $unit'_i = (x'_i, y'_i, r'_i, g'_i, b'_i)$
- 5 **for** $i = 0$ to $maxIter$ **do**:
- 6 $units \leftarrow unit'_i$
- 7 **if** $f(X) \neq f(X + units)$ **do**:
- 8 **break**
- 9 **end if**
- 10 **end for**
- 11 $X' = X + units$

V. EXPERIMENTAL EVALUATION

In this section, the experimental setup is introduced in Section A. We evaluate GreedyFool from the aspects of human eyes evaluation (Section B), perceptual distance results (Section C), misclassification ratio (Section D), fitness convergence (Section E) and the running time (Section F) on ResNet and DenseNet.

A. Experimental Setup

In this experiment, we implement GreedyFool in Python and conduct the adversarial example attack in CIFAR-10 over ResNet and DenseNet presented in Section II-A. Due to the size 32×32 and pixel value interval $[0, 255]$ of images, the population of the differential evolution is initialized by uniform distributions $U(1, 32)$ to generate x - y coordinate and Gaussian distributions $N(\mu = 128, \sigma = 127)$ for pixel RGB values. The fitness function of the differential evolution is set to pixel-wise objective function in Equation (15). The population size is 300 and the number of generations is 60. The weights of the channel modulation are fixed as $\{\chi_r = 0.299, \chi_g = 0.587, \chi_b = 0.114\}$ for all test images based on the RGB2GRAY conversion model. GreedyFool runs on an Intel Core i5 CPU 2.30 GHz, NVIDIA GeForce GTX 1060 and 8.0 GB of RAM computer running on Windows 10 and Spyder (Python 3.6).

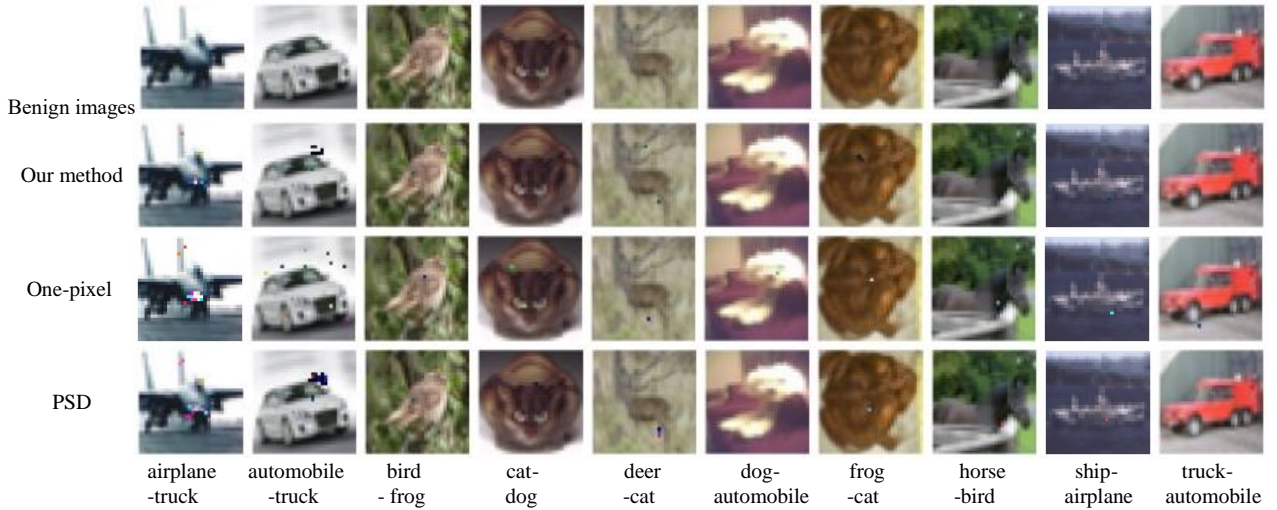


Fig. 6. Adversarial images synthesized by different attack methods against ResNet in CIFAR-10. Adversarial examples in the second row crafted by our method are much more imperceptible than others from the following rows.

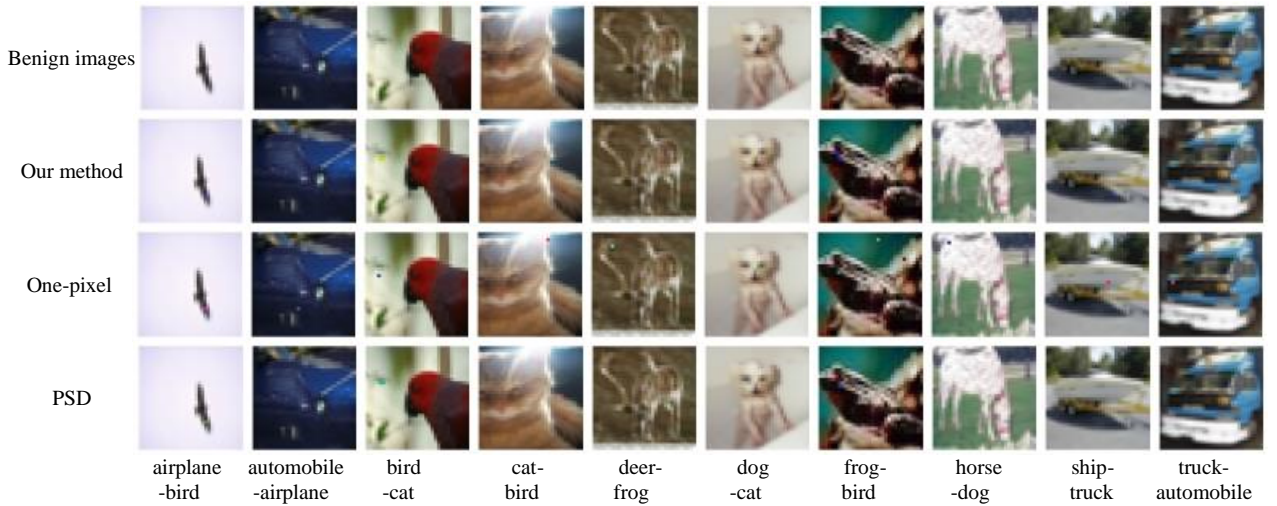


Fig. 7. Adversarial images synthesized by different attack methods against DenseNet in CIFAR-10. Adversarial examples in the second row crafted by our method are much more imperceptible than others from the following rows.

B. Human eyes evaluation

Like GreedyFool, both One-pixel attack [22] and PSD attack [31] belong to black-box attack using forward-propagation. Therefore, these three attacks are carried out on the same set of images to compare the imperceptibility of adversarial perturbations. We present 10 classes of images in Fig.6 and Fig.7, which include benign images and their corresponding adversarial images against ResNet and DenseNet. Adversarial examples from GreedyFool are listed in the second row. The following rows are adversarial examples synthesized by One-pixel attack and PSD attack.

Imperceptibility is the perceived response by human eyes caused by a physical stimulus, which is a subjective feeling varying with each individual. To evaluate the visibility of adversarial perturbations, we conduct extensive user study to design the scoring system based on human eyes evaluation. In this test, we recruit 60 participants to score the similarity between the benign images and the corresponding adversarial examples in Figures 6-7. For each trial, the benign images are shown on the screen at a fixed size and the order of adversarial images are random. The participants are required to give the score from 0 to 10 in 5 seconds. The higher score denotes the

more noticeable adversarial perturbations. A score of 0 means no difference, while a score of 10 means a complete difference. We calculate the average score for each class of images from human eyes evaluation and plot them in Fig.8 and Fig.9 for comparison.

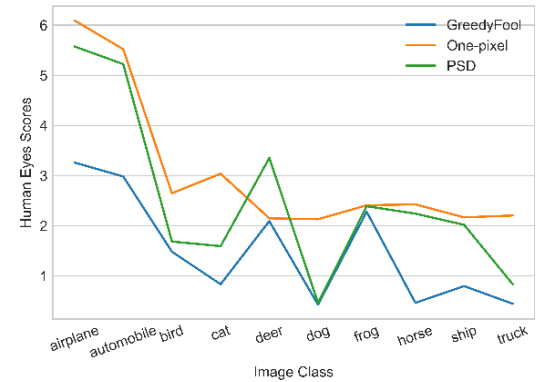


Fig. 8. Average scores comparison from human eyes evaluation between our attacks with existing attacks on ResNet.

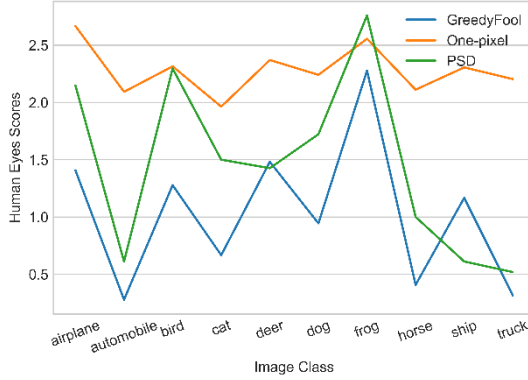


Fig. 9. Average scores comparison from human eyes evaluation between our attacks with existing attacks on DenseNet.

As shown in Fig.8 and Fig.9, GreedyFool has the lowest score in most classes, followed by PSD attack, and One-pixel attack has the highest score that human eyes easily detect the perturbed pixels. The results show that adversarial examples synthesized by GreedyFool are much more imperceptible than other pixel-wise methods, which are higher perceptual similarity to correspondingly benign images. Among the three types of attacks, One-pixel attack hardly takes the HVS into consideration. PSD attack considers the intensity and texture masking of benign images. GreedyFool combines JND,

Weber-Fechner law, texture masking with color channel modulation to construct objective function of adversarial example attacks, giving full consideration to the HVS. Human eyes experiment demonstrates that the imperceptibility of adversarial examples could be further improved by combining multiple HVS metrics.

C. Perceptual distance results

Imperceptibility refers to the indistinguishable distance by human eyes between benign examples and adversarial examples. The excellent perceptual distance should accurately reflect perceptual similarity between the benign example and the adversarial one. TABLE III lists *IntegLoss* results of adversarial examples generated by these three methods. The results show that GreedyFool could generate adversarial examples with smaller *IntegLoss* values than PSD attack and One-pixel attack, which are consistent with the scores from human eyes experiment in Section B.

TABLE IV lists the perceptual distance results of adversarial examples generated by GreedyFool in Fig.6 and Fig.7. The results show that L_p norms cannot always accurately quantify imperceptibility of adversarial perturbations. The proposed perceptual distance *IntegLoss* is a more accurate metric than L_p norms to reflect perceptual similarity between the benign example and the adversarial one.

TABLE III. THE PROPOSED PERCEPTUAL DISTANCE RESULTS OF ADVERSARIAL EXAMPLES IN FIGURES 6 AND 7

Networks	Method	airplane	automobile	bird	cat	deer	dog	frog	horse	ship	truck
ResNet	[22]	159.9725	680.6277	9.2656	7.4370	15.1543	8.9546	27.4190	16.3758	42.7534	23.9218
	[31]	49.3604	392.8105	6.0965	3.0108	23.1974	0.0123	12.1553	0.7286	3.1867	0.2651
	Our	35.6880	317.2337	2.9297	1.0145	25.5201	0.0027	11.4457	0.7147	3.0271	0.2397
DenseNet	[22]	2.9803	24.6410	11.0931	7.8807	7.3199	4.0381	10.8706	7.0604	13.9815	7.1886
	[31]	1.3220	0.0145	3.4483	2.4777	0.6707	0.5324	2.8408	0.2824	0.1785	0.1701
	Our	0.3427	0.0058	2.4050	0.6525	0.3950	1.0061	1.5546	0.1475	0.0397	0.0647

TABLE IV. THE PERCEPTUAL DISTANCE RESULTS OF ADVERSARIAL EXAMPLES IN THE SECOND ROW IN FIGURES 6 AND 7

Networks	perceptual distance	airplane	automobile	bird	cat	deer	dog	frog	horse	ship	truck
ResNet	L_0	11	16	1	1	2	1	1	1	1	1
	L_2	1871	5637	136	57	296	1	264	211	108	42
	L_∞	198	253	136	57	151	1	236	211	94	42
	<i>IntegLoss</i>	35.6880	317.2337	2.9297	1.0145	25.5201	0.0027	11.4457	0.7547	3.4271	0.2397
DenseNet	L_0	1	1	2	1	1	1	2	1	1	1
	L_2	210	2	397	125	69	93	462	75	5	47
	L_∞	210	2	203	125	69	72	247	75	5	47
	<i>IntegLoss</i>	0.3427	0.0058	2.4050	0.6525	0.3950	1.0061	1.5546	0.1475	0.0397	0.0647

D. Misclassification ratio

According to the purpose of tasks, adversarial example attacks could be classified as non-targeted attacks and targeted attacks. Non-targeted attacks aim to mislead DNN to classify images into any wrong classes, while targeted attacks aim to mislead DNN to classify images into a specific target class. The misclassification ratio is the most important property for adversarial example attacks. For non-targeted attacks, the misclassification ratio is formulated in Equation (16).

$$MR_{UA} = \frac{1}{N} \sum_{i=1}^N \text{count}(l \neq l') \quad (16)$$

where the function *count* is used to count the number of X' that is classified into the wrong class by deep learning. l and l' are labels of the benign example X and the adversarial on X' respectively. For targeted attacks, the misclassification ratio is formulated in Equation (17).

$$MR_{TA} = \frac{1}{N} \sum_{i=1}^N \text{count}(l = t) \quad (17)$$

where the adversarial example X' is classified into the target class t . we test 1000 random images and compare the misclassification ratio between GreedyFool and two previous works. The results demonstrate that GreedyFool achieves 100% success rate for non-targeted attacks and targeted attacks. In fact, when the perturbations are sufficient, any images could be recognized as a specified target class by deep learning. However, not all adversarial example attacks could achieve 100% success rate because some of them need to set the box-constrained parameters and generate adversarial examples under these constraints. For example, One-pixel attack [22] needs to specify the number of disturbed pixels and PSD attack [31] needs to set the max human perceptual distance D_{max} . When the number of disturbed pixels is set to 5, success rate of One-pixel attack achieve 86% for non-targeted attacks

and 44% for targeted attacks. When $D_{max} = 70$, success rate of PSD attack achieve 84% for non-targeted attacks and 72% for targeted attacks. However, the attacker cannot determine appropriate box-constrained parameters before adversarial example attacks on a specific image. The strict constraints may result in unsuccessful adversarial example attacks while the loose constraints may allow human eyes to detect the perturbations easily. GreedyFool utilizes the greedy approximation to obtain approximately the least visible perturbations without setting box-constrained parameters, which could automatically generate the imperceptible adversarial examples in 100% success rate.

E. Convergence of Fitness Function

The running speed of GreedyFool largely depends on the convergence of the differential evolution. The fitness function

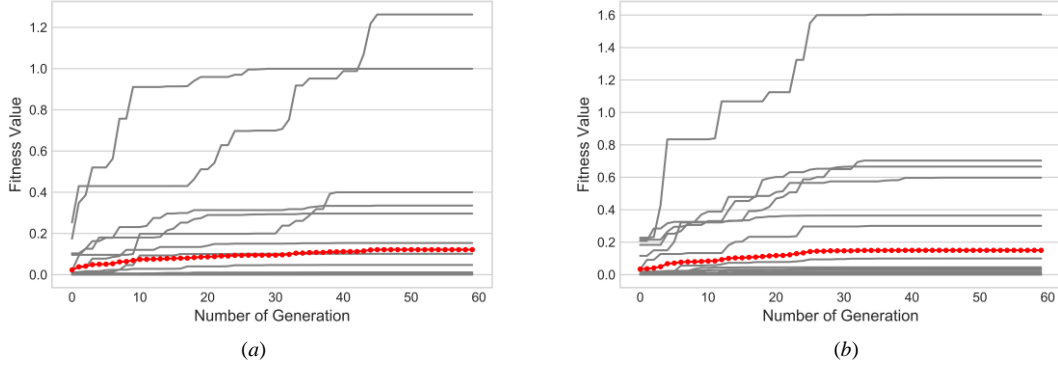


Fig. 10. Fitness convergence tests. (a) convergence of fitness function on ResNet, (b) convergence of fitness function on DenseNet. The average values are highlighted by red dotted lines.

F. Computation Cost

Computation cost refers to the running time for attackers to synthesize an adversarial example, which is used to evaluate the attack time cost. The computation cost of GreedyFool is affected by several factors, including the feedback time of the DNN model, convergence speed of the differential evolution, the number of the greedy approximation, running environment, etc.

The experiment chooses 30 random images from CIFAR-10 to test the actual running time of the DNNs and GreedyFool on these DNNs. The running time results of ResNet and DenseNet are plotted in Fig.11. The average running time of ResNet is 0.008346 seconds while that of DenseNet is 0.015876 seconds. The running time of DenseNet is significantly longer than that of ResNet. GreedyFool running time on ResNet and DenseNet is plotted in Fig.12. On average, GreedyFool takes about 14.943498 seconds on ResNet and 38.444529 seconds on DenseNet to synthesize an adversarial example. GreedyFool running time on DenseNet is significantly longer than that on ResNet.

The comparison between Fig.11 and 12 reveals that the running time of GreedyFool is not completely consistent with that of the corresponding DNN. But in general, because GreedyFool utilizes the feedback of the deep neural network to guide the evolution of the adversarial perturbations, its computation cost is closely related to the speed of the DNN. GreedyFool shows higher attack efficiency for such neural networks that can feedback probability labels in a short time.

is set to be the pixel-wise objective function called perturbation priority as defined in Equation (15). The goal of the differential evolution is to maximize this fitness value. We carry out fitness convergence tests on ResNet and DenseNet to observe how the fitness value changes during evolution. Figure 10 shows their fitness convergences of 30 random images during 60 generations.

As shown in Fig.10, each line plots the fitness convergence of an image. Some images could find the highest-priority perturbation pixel with a low number of generations, while others require a sufficient number of generations. Over both ResNet and DenseNet, the fitness function ends up being stable after about 50 generations. The results prove that the differential evolution is a feasible approach to solve for pixels with high perturbation priority.

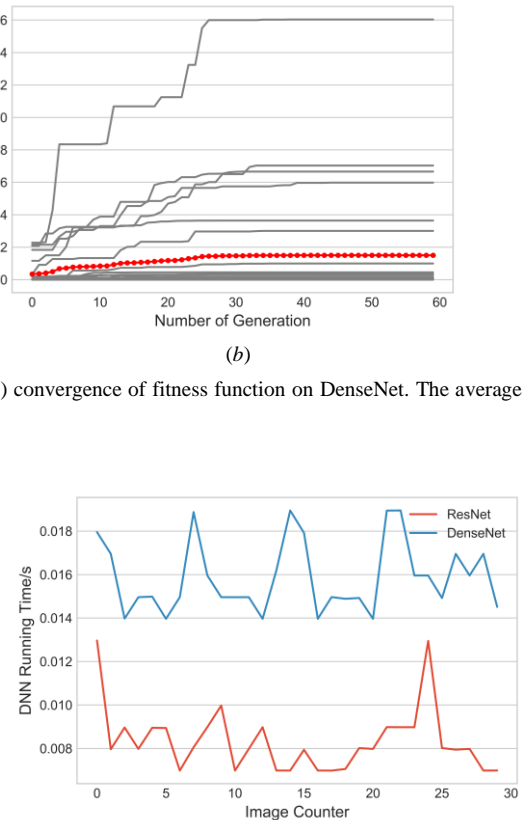


Fig. 11. The running time of ResNet and DenseNet for 30 random images.

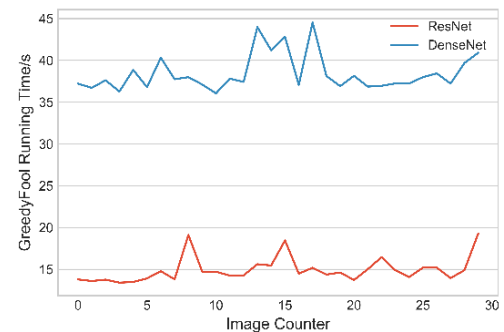


Fig. 12. GreedyFool running time for 30 random images over ResNet and DenseNet.

VI. DISCUSSION

In the paper, we propose a new adversarial example attack GreedyFool, which combines the differential evolution and the greedy approximation. The differential evolution is utilized to obtain a large number of candidates with high perturbation priority by generationally solving for optimization. Based on the greedy approximation, GreedyFool selects pixels with the current highest perturbation priority from candidates to synthesize adversarial examples until the successful attack. To sufficient imperceptibility, we launch investigations into the HVS and design an integrated metric considering JND, Weber-Fechner law, texture masking and channel modulation. GreedyFool has mainly the following remarkable properties:

(1) Black-box attack. GreedyFool attacks DNN models depending on only their probability labels but no inner information of target DNNs, such as gradients, network structures, etc.

(2) Imperceptibility. The definition of the perceptual loss takes JND, Weber-Fechner law, texture masking and channel modulation of the HVS into consideration, which introduces a comprehensive metric covering background luminance, nonlinear mapping of intensity, local texture feature and spectral sensitivity to evaluate the perceptual distance.

(3) Success rate. GreedyFool outperforms the state-of-the-art pixel-wise methods in the misclassification ratio, which achieves 100% success rate for both non-targeted attacks and targeted attacks.

(4) Flexibility. Rather than several gradient-based algorithms, the proposed algorithm based on differential evolution does not use the gradient information of neural network, so it can attack more types of DNN model even if their gradients are not differentiable.

(5) Automation. GreedyFool automatically synthesize the less perceptible adversarial examples based on the greedy approximation without setting box-constrained parameters.

VII. CONCLUSION

Adversarial example attacks against neural networks are a serious threat for the safety-critical systems. In this paper, we propose a novel approach GreedyFool to generate adversarial examples using forward-propagation. GreedyFool evaluates the effects of pixel-wise perturbations and generates the candidate pixels with the higher perturbation priority by the differential evolution. And the greedy approximation is used to get adversarial perturbations from candidates and automatically synthesize the imperceptible adversarial examples. GreedyFool could attack more types of DNNs depending on only their probability labels. In the definition of the perceptual loss, existing works lack sufficient consideration of the HVS, resulting in noticeable artifacts. We further launch a lot of investigations into the HVS and introduce an integrated metric to define the perceptual loss from background luminance, nonlinear mapping of intensity, local texture feature and spectral sensitivity. We implement GreedyFool and conduct the adversarial example attack in CIFAR-10 on ResNet and DenseNet. The experimental results demonstrate its much more imperceptibility than that of the state-of-the-art pixel-wise methods and its 100% success rate. Furthermore, we test the convergence of the fitness function and computation cost to prove the feasibility of GreedyFool.

REFERENCES

- [1] X. Yuan, P. He, Q. Zhu and X. Li, “Adversarial examples: Attacks and defenses for deep learning”, *IEEE Transactions on Neural Networks and Learning Systems*, vol. 30, no. 9, pp. 2805-2824, 2019.
- [2] K. He, X. Zhang, S. Ren, and J. Sun, “Deep residual learning for image recognition”, *IEEE Conference on Computer Vision and Pattern Recognition (CVPR)*, pp. 770-778, 2016.
- [3] G. Huang, Z. Liu, L. Maaten, and K. Weinberger, “Densely connected convolutional networks”, *IEEE Conference on Computer Vision and Pattern Recognition (CVPR)*, pp. 4700-4708, 2017.
- [4] S. Horiguchi, S. Amano, M. Ogawa and K. Aizawa, “Personalized classifier for food image recognition”, *IEEE Transactions on Multimedia*, vol. 20, no. 10, pp. 2836-2848, 2018.
- [5] X. Dong, J. Shen, D. Wu, W. Wang, and F. Porikli, “Quadruplet network with one-shot learning for fast visual object tracking”, *IEEE Transactions on Image Processing*, vol. 28, no. 7, pp. 3516-3527, 2019.
- [6] J. Li, S. Ji, T. Du, B. Li and T. Wang, “Textbugger: generating adversarial text against real-world applications”, *Network and Distributed System Security Symposium (NDSS)*, pp. 1-15, 2019.
- [7] T. Young, D. Hazarika, S. Poria and E. Cambria, “Recent trends in deep learning based natural language processing”, *IEEE Computational Intelligence Magazine*, vol. 13, no. 3, pp. 55-75, 2018.
- [8] Y. Qin, N. Carlini, G. Cottrell, I. Goodfellow and C. Raffel, “Imperceptible, robust, and targeted adversarial examples for automatic speech recognition”, *Proceedings of Machine Learning Research(PMLR)*, pp. 5231-5240, 2019.
- [9] A. Graves, A. Mohamed and G. Hinton, “Speech recognition with deep recurrent neural networks”, *IEEE International Conference on Acoustics, Speech and Signal Processing (ICASSP)*, pp. 6645-6649, 2013.
- [10] A. Chakraborty, M. Alam, V. Dey, A. Chattopadhyay, and D. Mukhopadhyay, “Adversarial attacks and defenses: a survey”. *arXiv preprint arXiv: 1810.00069*, 2018.
- [11] H. Xu, Y. Ma, H-C. Liu, D. Deb, H. Liu, J-L. T and A. Jain, “Adversarial attacks and defenses in images, graphs and text: a review”, *International Journal of Automation and Computing*, vol. 17, no. 2, pp. 151-178, 2019.
- [12] C. Szegedy, W. Zaremba and I. Sutskever, “Intriguing properties of neural networks”, *arXiv preprint arXiv: 1312.6199*, 2013.
- [13] I-J. Goodfellow, J. Shlens, and C. Szegedy, “Explaining and harnessing adversarial examples”, *arXiv preprint arXiv: 1412.6572*, 2014.
- [14] M. Sharif, S. Bhagavatula, L. Bauer L and M. Reiter, “Accessorize to a crime: real and stealthy attacks on state-of-the-art face recognition”, *ACM Conference on Computer and Communications Security (CCS)*, pp. 1528-1540, 2016.
- [15] H. Wang, D. Gong, Z. Li and W. Liu, “Decorrelated adversarial learning for age-invariant face recognition”, *IEEE Conference on Computer Vision and Pattern Recognition (CVPR)*, pp. 3527-3536, 2019.
- [16] E. Quiring, D. Arp and K. Rieck, “Forgotten siblings: Unifying attacks on machine learning and digital watermarking”, *IEEE European Symposium on Security and Privacy (EuroS&P)*, pp. 488-502, 2018.
- [17] J. Hayes, “On visible adversarial perturbations and digital watermarking”, *IEEE Conference on Computer Vision and Pattern Recognition Workshops (CVPR)*, pp. 1597-1604, 2018.
- [18] Z. Dou, S. Osher and B. Wang, “Mathematical analysis of adversarial attacks”, *arXiv preprint arXiv: 1811.06492*, 2018.
- [19] B. Rouani, M. Samragh, T. Javidi and F. Koushanfar, “Safe machine learning and defeating adversarial attacks”, *IEEE Symposium on Security and Privacy (S&P)*, pp. 31-38, 2019.
- [20] N. Papernot, P. McDaniel, I. Goodfellow, S. Jha, Z-B. Celik and A. Swami, “Practical black-box attacks against machine learning”, *ACM Conference on Computer and Communications Security (CCS)*, pp. 506-519, 2017.
- [21] N. Papernot, P. McDaniel, S. Jha, M. Fredrikson, Z-B Celik and A. Swami, “The Limitations of deep learning in adversarial settings”, *IEEE European Symposium on Security and Privacy (EuroS&P)*, pp. 372-387, 2016.
- [22] J. Su, D-V. Vargas and K. Sakurai, “One pixel attack for fooling deep neural networks”, *IEEE Transactions on Evolutionary Computation*, vol. 23, no. 5, pp. 828-841, 2019.

[23] S-M Moosavi-Dezfooli, A. Fawzi and P. Frossard, “Deepfool: a simple and accurate method to fool deep neural networks”, *IEEE Conference on Computer Vision and Pattern Recognition (CVPR)*, pp. 2574-2582, 2016.

[24] Y. Liu, X. Chen, C. Liu and D. Song, “Delving into transferable adversarial examples and black-box attacks”, *International Conference on Learning Representations (ICLR)*, pp. 1-14, 2017.

[25] N. Carlini and D. Wagner, “Towards evaluating the robustness of neural networks”, *IEEE Symposium on Security and Privacy (S&P)*, pp. 39-57, 2017.

[26] N. Carlini, G. Katz, C. Barrett and D-L. Dill, “Provably minimally-distorted adversarial examples”, *arXiv preprint arXiv: 1709.10207*, 2017.

[27] X. Yang, W. Ling, Z. Lu, E. Ong, and S. Yao, “Just noticeable distortion model and its applications in video coding”, *Signal Processing: Image Communication*, vol. 20, no. 7, pp. 662-680, 2005.

[28] Z. Wang, M. Song, S. Zheng, Z. Zhang, Y. Song and Q. Wang, “Invisible adversarial attack against deep neural networks: An adaptive penalization approach”, *IEEE Transactions on Dependable and Secure Computing*, DOI: 10.1109/TDSC.2019.2929047.

[29] J. Drosler, “An n-dimensional Weber law and the corresponding Fechner law”, *Journal of Mathematical Psychology*, col. 44, no. 2, pp. 330-335, 2020.

[30] S. Dehaene, “The neural basis of the Weber-Fechner law: A logarithmic mental number line”, *Trends in Cognitive Sciences*, col. 7, no. 4, pp. 145-147, 2003.

[31] B. Luo, Y. Liu, L. Wei and Q. Xu, “Towards imperceptible and robust adversarial example attacks against neural networks”, *AAAI Conference on Artificial Intelligence (AAAI)*, pp. 1-8, 2018.

[32] J-L. Schnapf, T-W. Kraft and D-A. Baylor, “Spectral sensitivity of human cone photoreceptors”, *Nature*, col. 325, no. 6103, pp. 439, 1987.

[33] Y. Song, L. Bao and X. Xu, “Decolorization: Is `rgb2gray ()` out?”, *International Conference on Computer Graphics and Interactive Techniques (SIGGRAPH)*, pp. 15, 2013.

[34] P. Civicioglu and E. Besdok, “A conceptual comparison of the cuckoo search, particle swarm optimization, differential evolution and artificial bee colony algorithms”, *Artificial Intelligence Review*, 2013: 1-32.

[35] X. Zhou, C. Peng, J. Liu, Y. Zhang and G-J Zhang, “Underestimation-assisted global-local cooperative differential evolution and the application to protein structure prediction”, *IEEE Transactions on Evolutionary Computation*, col. 24, no. 3, pp. 536-550, 2020.

[36] Z. Zhan, Z. Wang, H. Jin and J. Zhang, “Adaptive distributed differential evolution”, *IEEE Transactions on Cybernetics*, col. 10, pp. 1-15, 2019.